Experimental and Theoretical Investigation on the Catalytic Generation of Environmentally Persistent Free Radicals (EPFRs) from Benzene

Massimiliano D'Arienzo[*1], Livio Gamba[1], Franca Morazzoni[1], Ugo Cosentino*[*2], Claudio Greco[2], Marina Lasagni[2], Demetrio Pitea[2], Giorgio Moro[3], Cinzia Cepek [4], Valeria Butera[5], Emilia Sicilia[5], Nino Russo[5], Ana B. Muñoz-García[6], Michele Pavone[6].*

[1] INSTM, Department of Materials Science, University of Milano-Bicocca, Via R. Cozzi 55, I-20125 Milano, Italy

[2] Department of Earth and Environmental Sciences, University of Milano-Bicocca, Piazza della Scienza 1, I-20126 Milano, Italy

[3] Department of Biotechnology and Biosciences, University of Milano-Bicocca, Piazza della Scienza 2, I-20126 Milano, Italy

[4] Istituto Officina dei Materiali-CNR Laboratorio TASC, Strada Statale 14, km 163.4, I-34012 Trieste, Italy

[5] Department of Chemistry and Chemical Technologies, Università della Calabria, I-87036 Arcavacata di Rende, Italy

[6] Department of Chemical Sciences, University of Naples Federico II, Via Cintia 26, I-80126 Naples, Italy

ABSTRACT

Environmentally Persistent Free Radicals (EPFRs) are toxic products deriving from the incomplete combustion and are able to generate DNA damage and pulmonary dysfunction. They are formed on particulate matter through interaction with aromatic hydrocarbons, catalyzed by transition metal oxides, and produce reactive oxygen species (ROS) in aquatic media. The processes are already described for substituted aromatic molecules, e.g. phenol, not for unsubstituted aromatic systems, such as benzene.

The present paper reports on the reaction of benzene with molecular oxygen in the presence of Cu_xO/SiO_2, suggesting a mechanism based on cluster and periodic computational models. The activation of O_2 by interaction with silica coordinated Cu(I) centers leads to a peroxy species that yields the phenoxy radical upon reaction with benzene. Dissociation of $OH^{\bullet}$ radical eventually allows for the recovery of the catalyst.

The experimental characterization of the Cu_xO/SiO_2 catalyst regarded morphology, crystal structure, copper electronic state, and crystal field around Cu(II). Electron paramagnetic resonance (EPR) spectroscopy revealed the formation of phenoxy radical entrapped in the catalyst upon reaction between benzene and Cu_xO/SiO_2. Moreover, EPR investigation of ROS in aqueous solution evidenced the generation of $OH^{\bullet}$ radicals by benzene–contacted Cu_xO/SiO_2. All the experimental results nicely fit the outcomes of the computational models.

INTRODUCTION

Combustion and thermal processes are dominant sources of air pollution. These processes produce toxic products of incomplete combustion such as particulate matter (PM), polychlorinated dibenzo-*p*-dioxins and dibenzofurans (PCDD/Fs)[1-3], polycyclic aromatic hydrocarbons (PAHs)[4] and their derivatives, and environmentally persistent free radicals (EPFRs) [5-11].

EPFRs have been shown to generate DNA damage and induce pulmonary dysfunction associated with the free radical reactivity [6-11]. These adverse effects are believed to result from the onset of oxidative stress initiated by EPFRs and are consistent with the exposure to airborne fine and ultrafine particulate matter and smoking. EPFRs on PM are formed through the interaction of aromatic compounds with transition metal oxides (such as iron, copper, zinc, and nickel oxides) via surface mediated processes [12-16], as well as by interaction with neat silica or alumina surfaces[17, 18]. This results in the formation of surface-bound radical species which are stable enough to persist in the atmospheric environment for days, and which are also reactive in aquatic media to produce reactive oxygen species (ROS) [11]. The biological imbalance between the increase of ROS, like $OH^{\bullet}$, $^1O_2$, $O_2^{\bullet-}$, $HO_2^{\bullet}$, $HO_2^{\bullet-}$, H_2O_2, and the molecules that control the cellular homeostasis, leads to the oxidative stress, a process associated to respiratory and cardiovascular diseases [19, 20]. Specifically, ROS are thought to be able to induce different biological damages, from the simple inflammation to the more serious DNA damage [20-23].

Dellinger et al. [10] reported that EPFRs are formed after adsorption of substituted aromatic molecules such as phenols, chlorophenols and/or chlorobenzenes on the surface of CuO/SiO_2

highly porous catalyst, which simulates the PM particles, at temperatures between 100 and 400 °C. Depending on the nature of the aromatic precursor and substituents, and on the adsorption temperatures, some EPFRs as substituted phenoxy, catechoxy, and semiquinone radicals can be formed and they were detected by electron paramagnetic resonance (EPR) spectroscopy. These species then evolve and contribute to the ROS formation [11].

The generally accepted mechanism of EPFRs formation involves the chemisorption of chlorophenols and/or chlorobenzenes on the transition metal oxide. This induces an electron transfer from the organic adsorbate to the copper center, which results in the formation of the organic EPFR and in the reduction of the transition metal [10]. The EPFRs formation mechanism has been also theoretically investigated by density functional theory (DFT) calculations, studying the interaction of chlorophenols with Cu, CuO and Cu_2O surfaces [24-28].

Regardless of this background and even though strong EPR evidences support the generation of $PhenO^{\bullet}$ on copper oxide/silica surface by interaction of substituted aromatics, very few efforts have been devoted to deeply investigate the catalyst either as concerns on the morphological features (e.g. the particle size, the specific surface area, the copper clustering and distribution), or the variation of the metal center electronic state during the process [29].

Moreover, the literature on the EPFRs formation only evidences the reactivity of substituted oxo/halogenated benzenes [6-19, 30, 31], although benzene alone has been demonstrated to be highly active in inducing the generation of reactive oxygen species in biological systems [32]. Benzene metabolism is in fact a very complex process in which many enzymatic pathways lead to different metabolites linked to an enhanced ROS production [33]. Despite these outcomes, the

investigation of the interaction of benzene with the metal oxides contained in PM, the possible generation of EPFR and consequently of ROS, are still poorly investigated.

In the frame of industrial processes, the gas-phase oxidation of benzene with molecular oxygen, catalyzed by systems comparable to PM, i.e. Cu-supported zeolites, has been widely studied [33-38]. In this context Roduner *et al*. [38, 39], have recently followed by FTIR and EPR spectroscopies the direct hydroxylation of benzene to phenol, using Cu(II) impregnated zeolite as catalyst. The postulated mechanism firstly involves the Cu(II) reduction to Cu(I), the latter interacting with O_2 and producing EPR silent Cu(II)-O_2^- anions, which in turn activate the benzene ring oxidation [38]. This evidenced the essential role of Cu(I) in catalyzing the hydroxylation of benzene to phenol by interaction with molecular oxygen. The relation between the amount of Cu(I) sites and the yield of phenol formation catalyzed by copper-zeolites has been also evidenced by Tsuruya and Ichihashi in several studies [33-37]. Nevertheless, the mechanism proposed in these studies appears closely related to the peculiar zeolite structure and further efforts are required to analyze the behavior of benzene with copper oxide/silica. As far as the latter catalyst is concerned, it has been suggested [29] that copper(II) centers undergo partial reduction to Cu(I) during the vacuum annealing before the interaction with the organic contaminants and that benzene oxidation involves reduction of Cu(II) to Cu(I) centers [33-37]. Therefore, in the present investigation the EPFRs formation process will be studied referring also on the redox nature of the Cu_xO/SiO_2 (x = 1, 2) catalyst.

Based on the above state of art, the present study reports as a whole on the theoretical and experimental assessment of the EPFRs and ROS generation from benzene, catalyzed by copper-

containing silica, which simulates the PM particles. The computational approach is based on both cluster and periodic models, allowing us to propose a plausible pathway of benzene oxidation. The parallel EPR investigation gives evidence of the paramagnetic species (copper, EPFRs and ROS species) involved in the mechanism. Suggestions for the symmetry of the copper site have been also given. Besides, an in depth characterization of the particles size, the Cu_xO distribution and the copper oxidation states in the catalyst, has been performed, to identify possible connections among these features and the yield of EPFRs and ROS formation.

COMPUTATIONAL AND EXPERIMENTAL METHODS

1. Computational methods

Cluster model. All calculations were performed with the Gaussian 09 program [40]. Optimized geometries and harmonic vibrational frequencies of reactants, intermediates, products and transition states were calculated using the Density Functional Theory (DFT) with the hybrid functional B3-LYP [41-43] and the 6-311G** basis set. For Silicon and Copper atoms the LanL2 effective core potential and the related LanL2DZ basis set were used [44-46].

The nature of all the intercepted stationary points was confirmed by vibrational analysis. For all transition states it was carefully checked that the vibrational mode associated to the imaginary frequency corresponded to the correct movement of involved atoms. Spin-unrestricted calculations were performed for the radical systems. DFT densities and energies are known to be less affected by spin contamination than the corresponding unrestricted Hartree-Fock quantities [47].

Intrinsic Reaction Coordinate (IRC) calculations were used to link reactants and products with their transition states. All the energy values reported include electron energies and Zero Point Energy (ZPE) corrections.

Periodic model. Periodic spin-polarized Kohn-Sham density functional theory (DFT) were performed with the Vienna Ab-initio Simulation Package (VASP, version 5.3.5)[48] which features projected augmented-wave (PAW) potentials and plane-waves as basis set. The DFT+U approach was exploited with the exchange-correlation density functional of Perdew, Burke and Ernzenhof (PBE) [49, 50] and the rotationally invariant U-J formulation of Dudarev [51], with on-site corrections applied to the 3*d* manifold of Cu. A U_{eff}=U-J=6.0 eV, which was validated in previous works on bulk Cu_2O [52] was employed. The [Ar] core for Cu and [He] core for O have been replaced by PAW potentials from the VASP repository; for O that of standard hardness was used. With a kinetic energy cutoff for plane-waves equal to 600 eV and 3 x 3 x 1 Γ-centered k-point meshes, the total energies of our surface slab models (see below) converge up to 5 meV f.u.$^{-1}$ Adsorbates and reaction intermediates have been placed on one side of the slab and dipole corrections have been included accordingly.

2. Experimental methods

Synthesis of Cu_xO/SiO_2. Cu_xO/SiO_2 (x = 1, 2) powders were synthetized following the procedure previously reported by Dellinger et al [10]. The method is fast, but generally does not allow the control of the copper oxide loading and distribution in the final matrix. As in

particulate matter (PM) and fly ashes the metal oxides are randomly distributed, the synthesis was considered appropriate to reasonably simulate PM composition.

In brief, 5 mL of a 0.1 mol L^{-1} solution of copper nitrate trihydrate, $Cu(NO_3)_2 \cdot 3H_2O$, were added to 0.80±0.01 g of silica gel and left under magnetic stirring for 5 hours, casted into a Petri dish and then dried at 393 K overnight. The powders were then calcined in air at 723 K for 5 hours, using a temperature ramp of 5 K/min, collected, and finally ground in an agate mortar. Calcination in air leads to the formation of CuO and a very small fraction of Cu_2O onto the surface of silica gel particles (see XPS investigation).

The reactants amounts were chosen in order to obtain a catalyst nominally composed by 5 wt. % of CuO on silica.

Structural and morphological characterization. The actual Cu loading was determined by Inductively Coupled Plasma Atomic Emission Spectrometry (ICP-AES), using a using a PerkinElmer OPTIMA7000 DV spectrophotometer.

X-ray diffraction (XRD) patterns were collected with a Brucker D8 Advance (Cu K_α radiation) in the range 20-70° 2θ (2θ step 0.025°, count time of 2 s per step).

Scanning electron microscopy (SEM) measurements were performed by a Vega TS5136 XM Tescan microscope in a high-vacuum configuration. The electron beam excitation was 30 kV at a beam current of 25 pA, and the working distance was 12 mm. In this configuration, the beam spot was 38 nm. Prior to SEM analysis samples were gold-sputtered.

High-resolution transmission electron microscopy was performed using a Jeol 3010 apparatus operated at 300 kV with a high-resolution pole piece (0.17 nm point-to-point resolution) and equipped with a Gatan slow-scan 794 CCD camera. Samples were obtained by removing a film portion from the substrates in order to obtain a fine powder sample, then suspended in 2-propanol. A 5 μL drop of this suspension was deposited on a holey carbon film supported on a 3 mm copper grid for TEM investigation.

Nitrogen physisorption experiments were performed by using a Quantachrome Autosorb-1 apparatus. Specific surface area (SSA_{BET}) by the BET method and pore size distribution of mesopores by BJH method, were determined.

Spectroscopic characterization. The surface chemical composition of the Cu_xO/SiO_2 powders was investigated by X-ray photoelectron spectroscopy (XPS). Analysis was performed on as-prepared sample. The XPS spectra were acquired in ultrahigh vacuum (base pressure: ~ $1x10^{-10}$ mbar) at room temperature in normal emission geometry using a conventional Mg X-ray source ($h\nu$ = 1253.6eV) and a hemispherical electron energy analyzer (total energy resolution ~ 0.8eV). All binding energies (BE) are referred to the Fermi level. The standard deviation for the BEs values was ± 0.2 eV. Survey scans were obtained in the 0 – 1300 eV range. Detailed scans were recorded for the C1s, Si2p, O1s, and Cu2p regions. No further element was detected.

The fitting of the spectra involved a Shirley-type background subtraction and several Doniach-Sunjich components. Fitting parameters have been fixed according to Kaushik V. K. et al. [53] and taking into account the energy resolution used in the measurements (< 0.8 eV).

To study both symmetry and electronic state of copper centers supported onto silica, UV-Vis DRS spectra of carefully ground powders were recorded in the 800−200 nm range with a UV Lambda 900 PerkinElmer spectrophotometer, equipped with a diffuse reflectance accessory Praying Mantis sampling kit (Harrick Scientific Products, United States). A Spectralon disk was used as reference material.

EPR investigation. EPR studies of Cu_xO/SiO_2 samples were carried out using a Bruker EMX spectrometer operating in X-Band, with a frequency modulation of 100 kHz, 2-5mW of microwave power, magnetic field modulation of 2-5 Gauss and equipped with an Oxford cryostat operating in a range of temperatures between 4 and 298 K. Spectra on as-prepared samples were registered either at room temperature or at 130 K, mostly in static vacuum. Experiments aimed to detect EPFRs were performed in accordance with the Dellinger procedure [10].

In detail, a home-made contact system was utilized for the adsorption of molecular adsorbates onto the catalyst. The experimental setup consisted in a Schlenk-line connected both to vacuum and to inert gas (Ar), and provided by a pressure gauge. A tailor-made EPR reactor with the Cu_xO/SiO_2 sample, and a reservoir reactor containing the pollutant (benzene) were connected to the line. Before any experiment, the system was evacuated down to $p < 10^{-1}$ mbar, in order to avoid any possible contamination.

For the contact, about 150 mg of Cu_xO/SiO_2 powders were charged in the EPR reactor. The system was then evacuated at $p < 10^{-1}$ mbar and simultaneously heated up to 503 K. Cu_xO/SiO_2 was successively contacted for 10 minutes at the same temperature with p = 20 mbar of Ar

saturated with benzene. After exposure, the sample was again evacuated down to $p < 10^{-1}$ mbar for 1h at the dosing temperature to remove any residual physisorbed dosant.

In order to demonstrate the involvement of EPFRs in ROS production, spin-trap experiment on Cu_xO/SiO_2 samples either pristine or contacted with benzene were performed, following a previously reported procedure.

In detail, 1 mg/mL suspensions were prepared in PBS (phosphate buffer solution) and then sonicated for 5 minutes. Oxygen was bubbled into the suspensions for 5 minutes and ultrasound was applied again. Finally, an aliquot of each suspension was charged in a 250 μL EPR flat cell and the spectrum was recorded at 298 K. Instrumental conditions for the experiments were: Receiver Gain 2.52 x 10^5, Mod. Amplifier 2.000 G, Center Field 3505.180 G, Sweep Width 100.000 G, Time Constant 40.960 ms, Conversion Time 10.240 ms and Sweep Time 20.972 s, 50 accumulations.

RESULTS AND DISCUSSION

1. Computational results

Several evidences [36-40] highlight the role of Cu(I) in promoting benzene oxidation to phenol, but it is still lacking a mechanism at molecular level which takes into account all the observed results: the activation of molecular oxygen by Cu(I) sites, the oxidative step of the aromatic system, the stabilization of the phenoxy radical and the restoration of the Cu(I) catalytic site.

In order to propose a complete mechanism, our theoretical investigation was carried out by means of two different models of the Cu(I) sites, representing the two possible extreme conditions in which Cu(I) centers lie in Cu_xO/SiO_2. The first model mimics the case of totally dispersed metal centers on silica and consists of a molecular cluster having one Cu(I) embedded in the silica matrix. The second one assumes a whole crystalline surface of Cu_2O and makes use of a periodic approach. Of course, in the operative conditions hydration of the surface can occur and Cu centres will be partially hydroxylated. However, here a totally de-hydrated surface has been considered, to focus on the reactivity of those Cu(I) centres most prone to O_2 binding.

Cluster Model. In order to model the dispersed copper centers on silica, we assumed the simple cluster model $[Cu(Si_4O_{12}H_6)]^{-1}$ (Scheme 1), that includes one Cu(I) coordinated to two oxygen atoms of the silica. This kind of models have been successfully applied to the reactivity investigation of low valent silica coordinated Cu centers [54, 55].

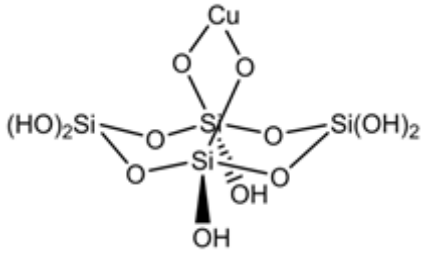

Scheme 1

Table 1 reports the relative energies, including electron energies and Zero Point Energy (ZPE) corrections, for intermediates and transition states involved in the proposed mechanism (Figure 1); Table 2 reports significant bond lengths (Å) for involved molecular species; Table 3 reports

Mulliken spin populations and charges of selected fragments composing the various species. The initial step of such mechanism involves the activation of molecular oxygen (in its $^3\Sigma_\gamma$ state) due to interaction with Cu(I) metal center.

The copper center interacts *end on* or *side on* with molecular oxygen providing the Cu(II)-oxygenated intermediates **A1** or **B1**, which are, respectively, 7.9 and 4.5 kcal mol^{-1} more stable than the reference, i.e. the separated reactants. In **A1,** the O_a-O_b bond distance, equal to 1.206 Å in an isolated O_2 molecule, increases up to 1.294 Å, and the spin population on O_2 is equal to 1.47 spin units. In **B1** the O_a-O_b bond distance is equal to 1.239 Å, and the spin population on O_2 is equal to 1.71 spin units.

The approach of a benzene molecule to the catalytic site via a barrier-less physical adsorption process provides the **A2** adduct, 12.5 kcal mol^{-1} more stable than the reference, and in which the oxygen coordination was found to be exclusively side on.

Successively, the reaction provides the **A3** intermediate where the C_a-O_a bond between an aromatic carbon atom and one of the oxygen atoms bonded to the copper ion is formed. The barrier for **A3** formation is 37.3 kcal mol^{-1}. This intermediate results 23.7 kcal mol^{-1} less stable than the reference and it presents almost one unpaired electron (0.94 spin units) delocalized on the phenyl ring. The O_a-O_b bond distance further increases up to 1.443 Å.

A3 easily interconverts into **A4** by torsional rotation around the Cu-O_b bond (energy barrier: 0.9 kcal mol^{-1}) and consequent breaking of the Cu-O_a bond. This intermediate presents the same stability (23.8 kcal mol^{-1} with respect to the reference) and spin population on the phenyl ring (0.94 spin units) as compared to **A3**. In **A4** the O-O bond distance is equal to 1.416 Å.

In the next step, **A4** undergoes a hydrogen transfer reaction: the H_a atom originally bonded to C_a moves to O_b. The energy barrier involved in this step is equal to 32.3 kcal mol^{-1}. In the transition state (TS) the distance between H_a and C_a is as long as 1.566 Å, whereas the H_a-O_b distance is 1.209 Å. Most interestingly, in the TS the O_a-O_b bond distance increases up to 1.502 Å: as a consequence, in the product we predict the complete breaking of the O-O bond and, concomitantly, the binding of the resulting phenoxy moiety to the copper ion yielding the **A5** intermediate. [FootNote: Interestingly, the **A5** intermediate can also derive directly from **A3**, as a result of transfer of H_a to O_b and simultaneous breaking of the O_a-O_b bond: the involved barrier is 31.4 kcal mol^{-1}, to be compared to the barrier involved in the A4-A5 interconversion (32.3 kcal mol^{-1}).] Noticeably, **A5** is 46.1 kcal mol^{-1} more stable with respect to the reference. Moreover, for this intermediate both a triplet state and a biradical singlet state, featuring antiferromagnetic coupling, turned out to be possible with comparable stability, as shown by the results of broken symmetry calculations (see Supporting Information).

Breaking of the Cu-O_a bond in **A5** is associated with a low barrier (1.9 kcal mol^{-1}) and leads to the formation of the **A6** van der Waals adduct, 49.9 kcal mol^{-1} more stable with respect to the reference.

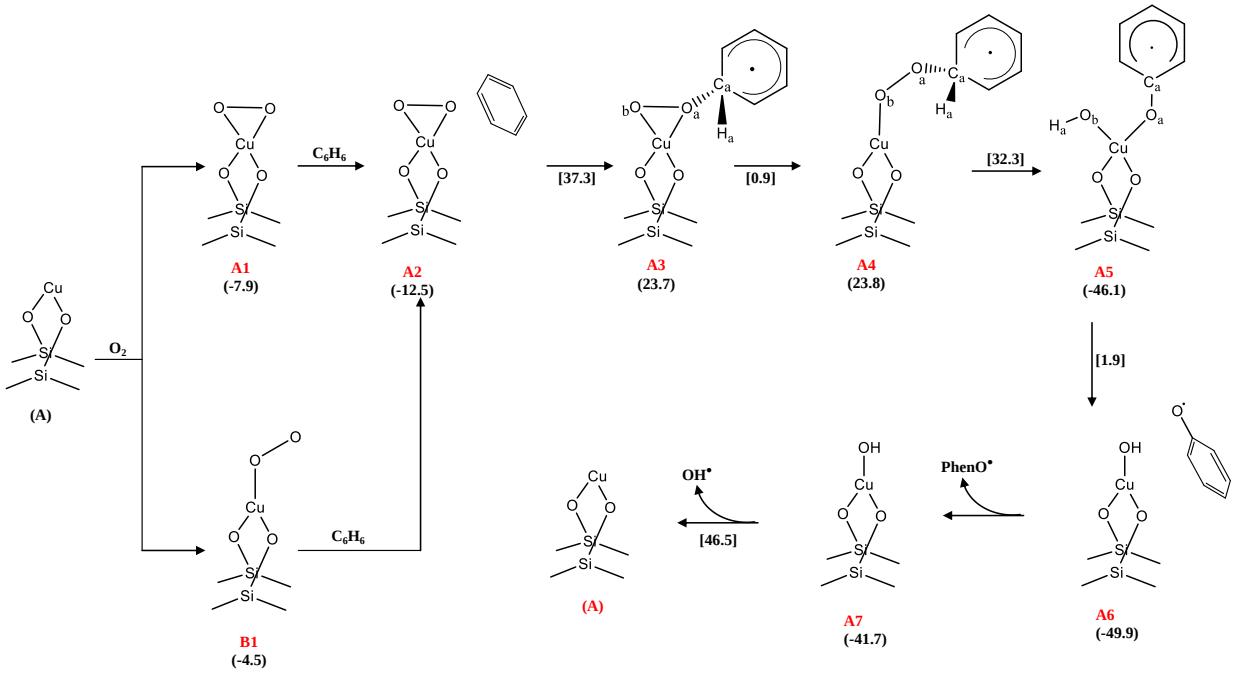

Figure 1. Mechanism of benzene hydroxylation activated by $[Cu(Si_4O_{12}H_6)]^{-1}$ catalyst: we report the reaction scheme, the relative electron energies of intermediates with respect to separate reagents (round parentheses), and the activation energies (square parentheses). Reported energies include Zero Point Energy corrections. Unpaired electrons are explicitly represented only when localized on the free hydroxyl or on the organic moieties.

Table 1. B3-LYP relative energies calculated with respect to the reagents species ($A+O_2+C_6H_6$) for intermediates and transition states involved in benzene hydroxylation catalyzed by **A**. Energy values include electron energies and Zero Point Energy (ZPE) corrections.

	Relative energies (kcal mol^{-1})	Energy barriers (kcal mol^{-1})
A + $^3O_2$ + C_6H_6	0	-
A1 + C_6H_6	-4.5	-
B1 + C_6H_6	-7.9	-
A2	-12.5	-
TS-**A2A3**	24.8	37.3
A3	23.7	-
TS-**A3A4**	24.6	0.9
A4	23.8	-
TS-**A4A5**	56.1	32.3
A5	-46.1	-
TS-**A5A6**	-44.2	1.9
A6	-49.9	-
A7 + $C_6H_5O^{\bullet}$	-41.7	-
A + $C_6H_5O^{\bullet}$ + $^{\bullet}OH$	4.8	-

Table 2. Selected bond lengths (Å) for molecular species involved in benzene hydroxylation catalyzed by **A**.

	O-O	Cu-O_a	Cu-O_b	O_a-C_a
A1	1.294	2.067	2.067	
B1	1.239	-	2.037	
A2	-	-	-	
TS-**A2A3**	1.396	2.203	1.927	1.671
A3	1.443	2.198	1.919	1.481
TS-**A3A4**	1.430	2.455	1.882	1.474
A4	1.416	-	1.867	1.471
TS-**A4A5**	1.502	-	1.917	1.438
A5	-	2.199	1.853	1.261
TS-**A5A6**		3.325	1.819	1.255
A6	-	-	-	
A7	-	-	2.037	
O_2	1.206			
$C_6H_5O^{\bullet}$	-	-	-	1.252

Table 3. Mulliken spin populations and charges of selected fragments composing the various species involved in benzene hydroxylation catalyzed by **A**.

	$Cu(Si_4O_{12}H_6)$		Cu		O_2		C_6H_6		$C_6H_5O^{\bullet}$		$OH^{\bullet}$	
	charge	Spin pop.	charge	Spin pop.	charge	Spin pop.	charge	Spin pop.	charge	Spin pop.	charge	Spin pop.
A	-1.000	0.000	0.232	0.000								
A1	-0.664	0.526	0.692	0.405	-0.336	1.474						
B1	-0.823	0.290	0.487	0.238	-0.177	1.710						
A3	-0.651	0.637	0.683	0.506	-0.620	0.423	0.271	0.940				
A4	-0.623	0.623	0.702	0.490	-0.612	0.435	0.235	0.942				
A5	-0.712	0.728	0.672	0.594					0.088	1.001	-0.375	0.271
A7	-0.596	0.777	0.726	0.602							-0.404	0.223

Dissociation of **A6** yields the phenoxy radical and **A7**, these intermediates being 41.7 kcal mol^{-1} more stable with respect to the reference. Mulliken spin population analysis shows the presence of one unpaired electron on the **A7** species, mostly localized on the Cu center (0.60 spin units). Finally, in the last step, the catalytic cycle is closed by dissociation of the hydroxyl radical, with an energetic cost of 46.5 kcal mol^{-1}. The overall reaction energy for the phenoxy and hydroxyl radicals formation from benzene and molecular oxygen is mildly endoenergetic by 4.8 kcal mol^{-1}.

Periodic Model. To model the reactivity of a Cu-rich region of the catalyst with more than a single isolated Cu(I) center, a periodic approach was employed, exploiting the $Cu_2O(111)$ surface slab as depicted by Figure 2 (see Supporting Information for convergence tests as a function of the number of O-Cu-O tri-layers). In this model the surface lattice vectors have been determined from the PBE+U optimized Cu_2O bulk lattice (u=v=6.065 Å, γ=120°). Moreover a vacuum layer between surfaces greater than 18 Å has been included to prevent interactions between periodic images along the direction perpendicular to the surface (c axis).

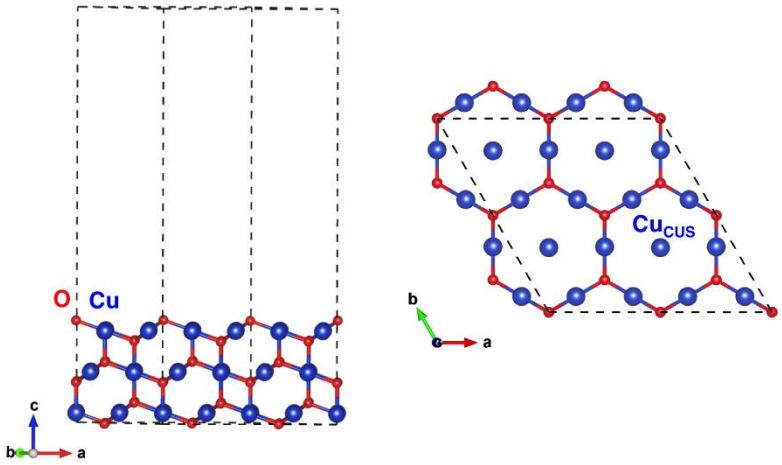

Figure 2. Left: $Cu_2O(111)$ periodic slab model containing three O-Cu-O tri-layers with a lateral periodicity of (2x2), corresponding to 4 surface unsaturated Cu (Cu_{CUS}) atoms per supercell. Blue spheres represent Cu and red spheres represent O atoms. Right: top view of the first O-Cu-O tri-layer.

The energetics of the reaction intermediates on this highly reactive Cu_2O (111) surface has been studied following the reaction path described in Figure 1. In this surface, adsorption of the O_2

molecule occurs preferentially through **B1** intermediate (E_{ads} =-24.5 kcal mol^{-1}), while **A1**-like adsorption is not stable; the system relaxes to either **B1** or a Cu_{CUS}-O_b-O_a-Cu bridge-like structure "**C1"**, slightly higher in energy than **B1** (E_{ads} = -24.4 kcal mol^{-1}). In terms of reactivity, **C1** is equivalent to **B1** since both relax to **A4**. In **B1**, the Bader charge analysis shows that the O_2 is activated by receiving 0.41 e^-; 0.25 e^- are donated by coordinating Cu_{CUS}, while the remaining 0.16 e^- are a contribution of the whole Cu sublattice. This results in an elongation of the O-O bond distance of 0.11 Å.

Activated adsorbed O_2 engages the benzene ring to form **A4** intermediate with a cost of 23.9 kcal mol^{-1}. In this structure, the O-O distance increases up to 1.439 Å. Our calculations indicate that the benzene ring donates around 0.5e^- to the O_2 moiety. Transfer to the surface of the non-planar hydrogen atom within the C_6H_6 ring is quite favored on the surface due to the formation of Cu-O_b(OH)-O_a(OPh)-Cu **A5** structure, wherein the latter, Cu_{CUS} is formally tri-coordinated but, practically, share the two adsorbates with ring-like Cu atoms. Moreover, in **A5** the O-O distance is 2.830 Å, which corresponds to the the O-O bond breakage .

Analysis of the electronic structure shows the presence of spin density on the adsorbed O_2 molecule (**B1**); as depicted in Figure 3, this spin density is delocalized to the benzene ring across the reaction path, through **A4** up to the formation of the metal-coordinated phenoxy radical (**A5**). For all previous steps, inclusion of vdW dispersive forces via the DFT-D3(BJ) approach, does not change the qualitative picture of the reaction mechanism (see Figure S1 in Supporting Information).

Overall, the periodic PBE+U calculations confirm the general scheme proposed with cluster calculations, where one active Cu(I) species is the main center for the interaction with the oxygen molecule and the formation of the peroxy radical (see Figure S1 in Supporting Information).

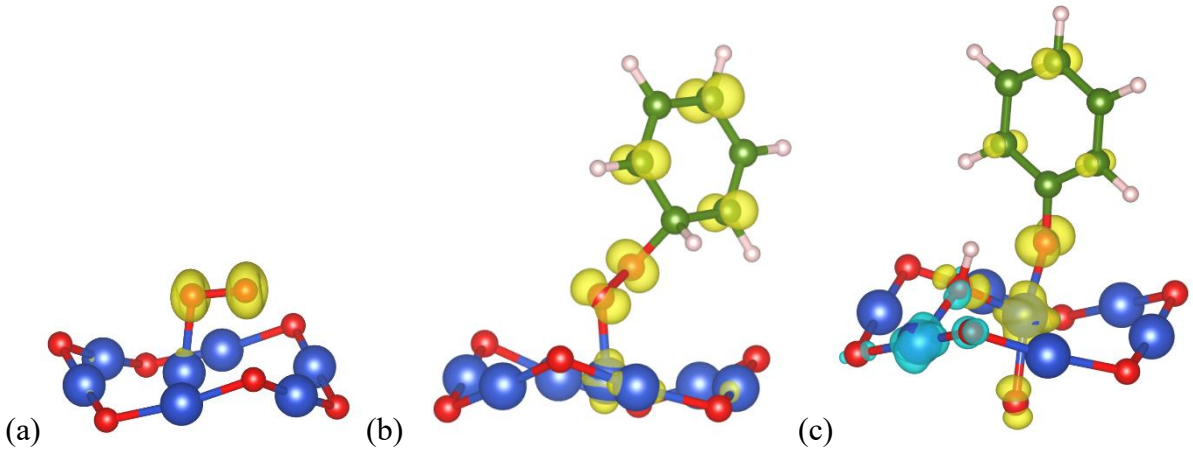

Figure 3. Computed electron spin density iso-surface plots of (a) O_2 molecule adsorbed on Cu_2O (111) (**B1**), (b) **A4** and (c) **A5** intermediates adsorbed on $Cu_2O(111)$. Only Cu_{CUS} and surrounding Cu_2O ring are shown for clarity. Yellow and cyan densities represent positive and negative spin values, respectively (iso-surface value = 0.025).

2. Experimental results

Structural and morphological characterization of Cu_xO/SiO_2 catalyst. Before any reactivity test, Cu_xO/SiO_2 has been deeply characterized as from the compositional, structural and morphological point of view.

In detail, ICP-AES analysis attested that the copper loading corresponds to 1.88±0.02 wt. %, i.e. a value significantly lower than the nominal one (5 wt.%). It is noteworthy that the determined copper content lies within the loading range of a previous study regarding the effect of CuO loading on EPFRs formation from substituted phenols [7].

The structural features of Cu_xO/SiO_2 were investigated by XRD diffraction. Figure 4 shows the XRD pattern of the as-synthesized powders. The diffraction peaks have been indexed based on the monoclinic crystal system with space group *C*2/*c*.

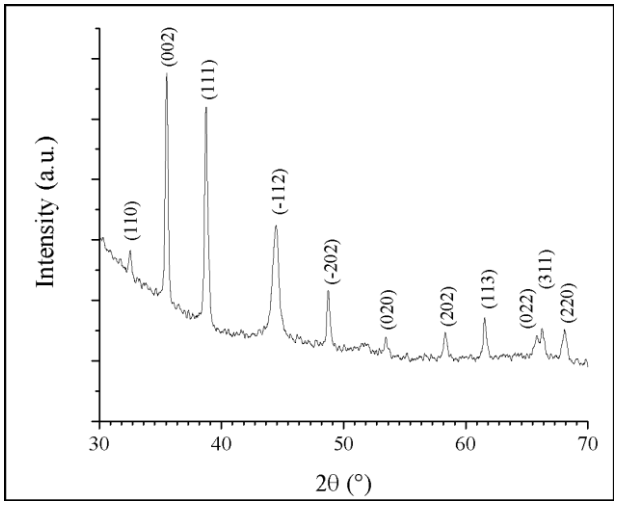

Figure 4. XRD pattern of Cu_xO/SiO_2 sample. All the reflections on the pattern can be indexed as monoclinic CuO phase with lattice constants comparable to the reported data (JCPDS 05-0661).

Compared with the standard diffraction pattern of CuO (JCPDS Card No. 05-0661), no other peaks belonging to crystalline impurities, such as $Cu(OH)_2$ or Cu_2O are detectable. Nonetheless, the presence of an amorphous phase, related to the silica particles, can be appreciated from the increase of the background intensity at small angles in the diffractogram.

The morphology of Cu_xO/SiO_2 and the copper distribution were preliminarily studied by SEM microscopy. In detail, SEM micrographs showed that Cu_xO/SiO_2 is constituted by micrometric silica agglomerates (length > 100 μm) with almost irregular shape, uniformly decorated by CuO nanoaggregates (Fig. 5 a-c). In particular, elemental mapping of Cu obtained by SEM-EDX evidenced a rather homogeneous distribution of copper on silica surface (Fig. 5d).

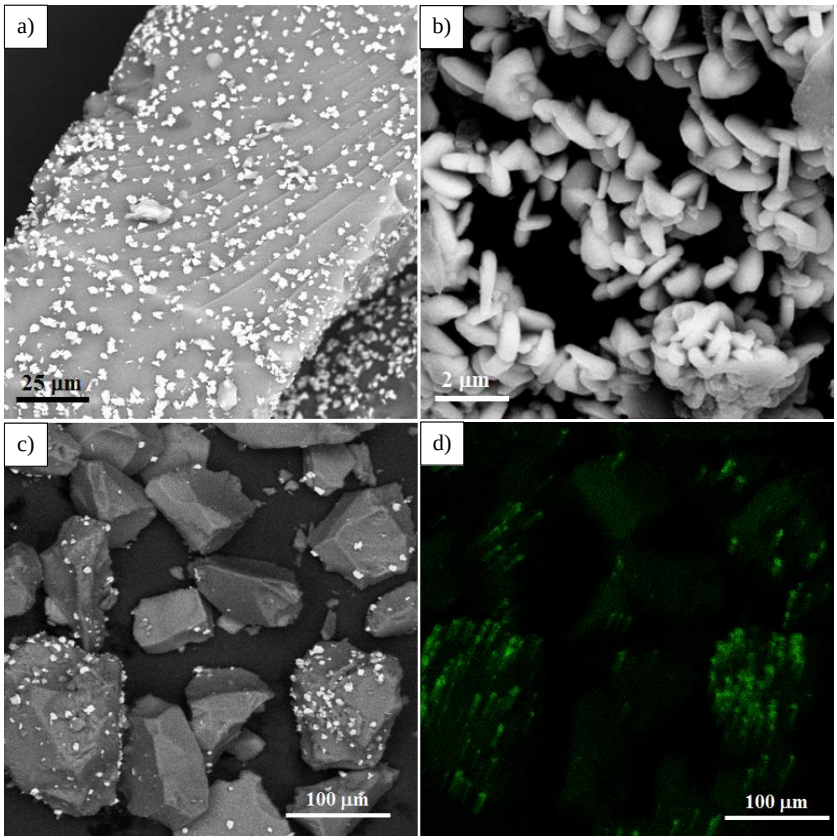

Figure 5. a), b) and c) SEM micrographs at different magnifications of Cu_xO/SiO_2 particles. d) Elemental mapping of Cu in the region described by figure c).

In order to gain deeper insight into the morphological features of Cu_xO/SiO_2, TEM investigation was carried out. The images revealed that SiO_2 agglomerates are actually composed by small irregularly shaped nanoparticles with average length 10-20 nm (Fig. 6a and b). Moreover, the amorphous nature of the support and the porosity of the system are also appreciable.

High resolution images (HRTEM), allowed to identify almost spherical CuO nanocrystals (average diameter ~ 5 nm) with well detectable crystallographic planes, anchored to the silica surface and often forming aggregates of larger dimensions (Fig. 6c and d).

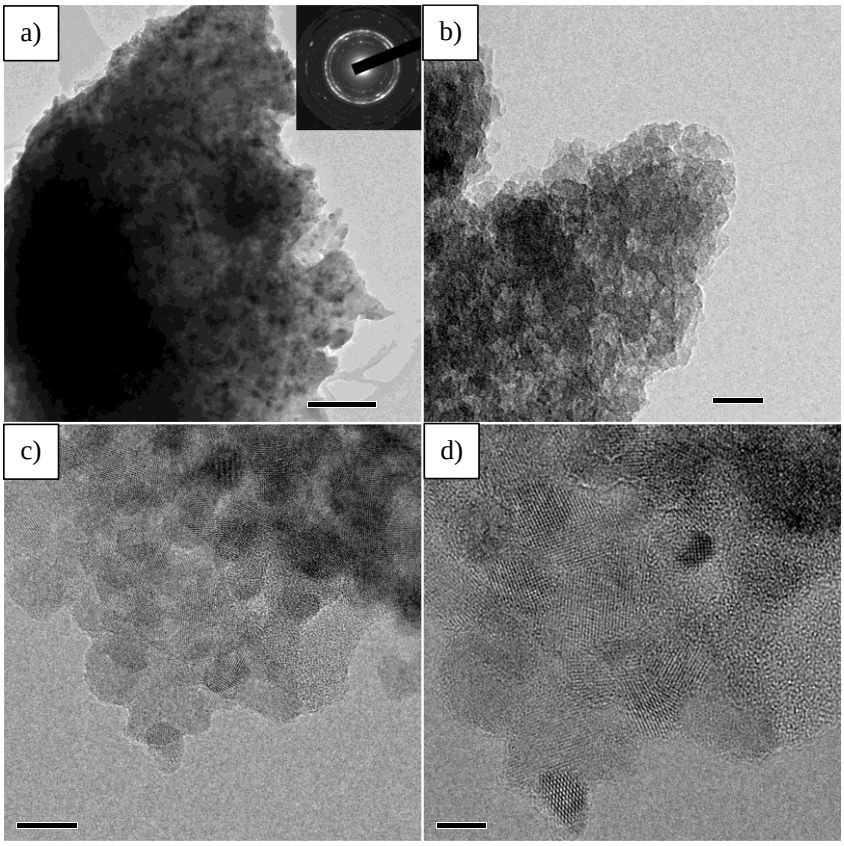

Figure 6. a) and b) TEM images of Cu_xO/SiO_2 sample. c) and d) HRTEM images highlighting the crystalline nature of the CuO nanoparticles anchored on the surface of amorphous silica.

As the knowledge of the specific surface area, the pore size and volume are key parameters to control the catalytic activity, nitrogen physisorption experiments were performed on both bare silica gel calcined at 723 K or Cu_xO/SiO_2 particles.

Both samples are mesoporous and show a type IV Brunauer isotherm (Fig. 7) and monomodal pore size distributions centered at ~ 5 nm (insets in Fig. 7). According to the t-plot, no micropores were detected. The obtained specific surface areas (SSA_{BET}) and BJH pore volumes are reported in Table 4. The results indicate a high porosity for both the systems even if, after copper impregnation, a decrease of specific surface area and pore volume of the silica powders was observed. This may be likely attributed to the presence of CuO nanocrystals, which tend to occlude the small mesopores, thus reducing the whole pore volume and the total surface area of the silica gel.

In summary, morphological investigation unveiled the importance of achieving a homogeneous copper distribution onto the surface of micrometric silica agglomerates, avoiding excessive clustering of the metal in large aggregates. Moreover, the large specific surface area of the catalytic system assessed by nitrogen physisorption experiments is a key parameter to promote an enhanced adsorption of the organic pollutants and, in turn, the generation of EPFRs.

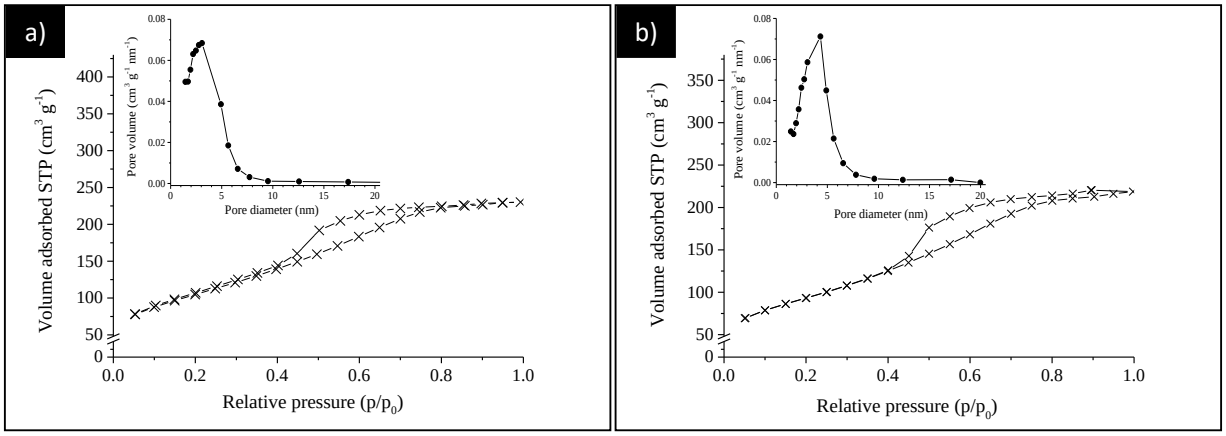

Figure 7. Adsorption/desorption isotherm at liquid nitrogen temperature for a) Silica gel calcined at 723 K and b) Cu_xO/SiO_2 sample. The curves correspond to a type IV isotherm with capillary condensation in the mesopores. Insets: pore size distributions.

Table 4 – SSA_{BET} and Pore Volumes determined for silica gel calcined at 723 K and Cu_xO/SiO_2 particles

Sample	**SSA_{BET} (m^2/g)**	**Pore Volume (cm^3/g)**
Silica gel	380.3±7.6	0.400
Cu_xO/SiO_2	335.9±6.7	0.339

Spectroscopic characterization of Cu_xO/SiO_2. In order to investigate the copper species, which promote the benzene oxidation, the surface composition of the Cu_xO/SiO_2 was studied by XPS. The binding energies (BE) values were measured for the Si2p, O1s, Cu2p and C1s lines. The nature of the O1s peak (BE = 530.5 eV) supports the formation and chemical stability of copper oxides for all the samples.

Figure 8 shows the XPS spectrum of Cu_xO/SiO_2 in the Cu $2p_{3/2}$ region.

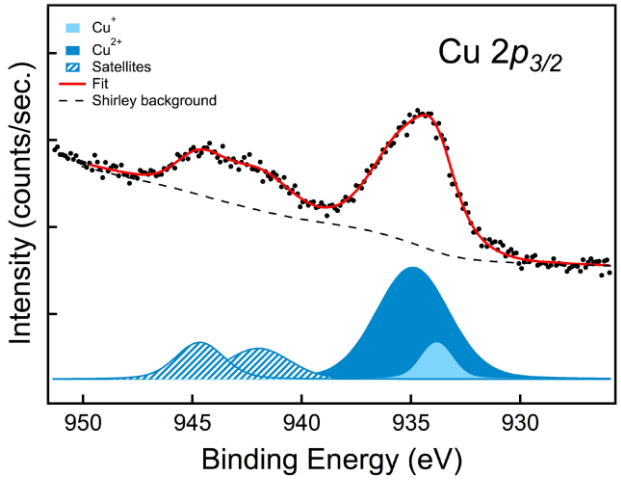

Figure 8. Cu $2p_{3/2}$ XPS spectrum (dots) of the Cu_xO/SiO_2 matrix.

The spectrum has been reproduced by fitting the experimental data (dots) using a Shirley background (dotted line) and several Doniach-Sunjich components. The main component (dark blue) at a binding energy of ca. 934 eV is consistent with the presence of the Cu(II) centers of CuO [56]. The weaker component (light blue) at a lower binding energy (< 932.5 eV) is instead attributable to Cu(I) species [56]. The satellite peaks at ca. 942 and 945 eV associated with these oxidation states, are also prominent (striped curves).

By supposing a homogeneous stoichiometry, XPS indicates that the whole copper amount is ~1 atomic % with respect to Si and Cu (I) accounts for about the 10% of the total amount of Cu.

In order to understand the electronic and coordination properties of silica-supported copper centers, the UV-Vis DRS spectrum of Cu_xO/SiO_2 was recorded before benzene contact and compared with that of bare silica calcined at 723 K (Fig. 9).

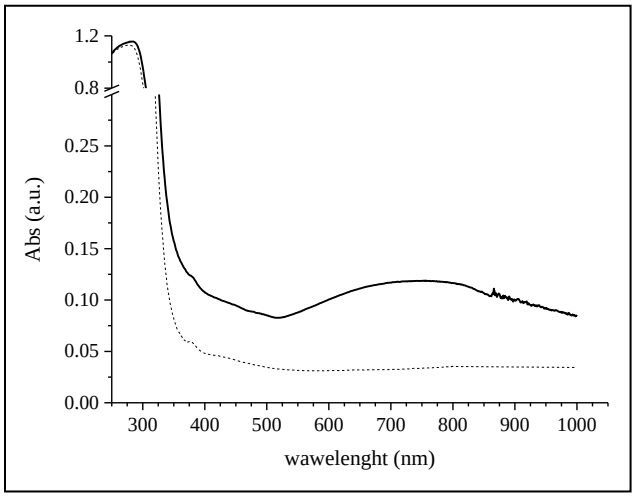

Figure 9. UV-Vis DRS spectra of silica gel calcined at 723 K (dashed line) and Cu_xO/SiO_2 (black-bold line).

A broad band, probably the superimposition of several absorptions, with a maximum around 750 nm was observed. The shape and the energy of this band are slightly different from those observed in pure CuO and may be assigned to d-d transitions of Cu(II) centers in a highly distorted pseudo-octahedral coordination [57].

Due to their low amount and the absence of active d-d transitions, Cu(I) centers cannot be detected. After contact with benzene no spectrum modifications were evident.

EPR investigation: study of EPFRs and ROS generated by Benzene on Cu_xO/SiO_2.

EPR evidences support in literature the generation of EPFRs, due to chemisorption of chlorine- and hydroxy-substituted benzenes on Cu_xO/SiO_2 surface, and their involvement in the subsequent formation of ROS [10, 11]. Nevertheless, the reactivity of the much more stable benzene in the presence of copper-containing oxide particles, still represents a matter of investigation.

Here, the interaction of benzene with Cu_xO/SiO_2 has been studied by EPR in order to provide experimental evidences of the theoretical mechanism in Figure 1, where Cu(I) center promotes the activation of chemisorbed molecular oxygen forming the Cu(II)-O_2^- [38]. This latter species attacks the stable aromatic ring, resulting in the formation of the PhenO$^\bullet$ radical.

As a first step, the spectromagnetic properties of copper centers in Cu_xO/SiO_2 before the interaction with benzene have been investigated in depth (Fig. 10)

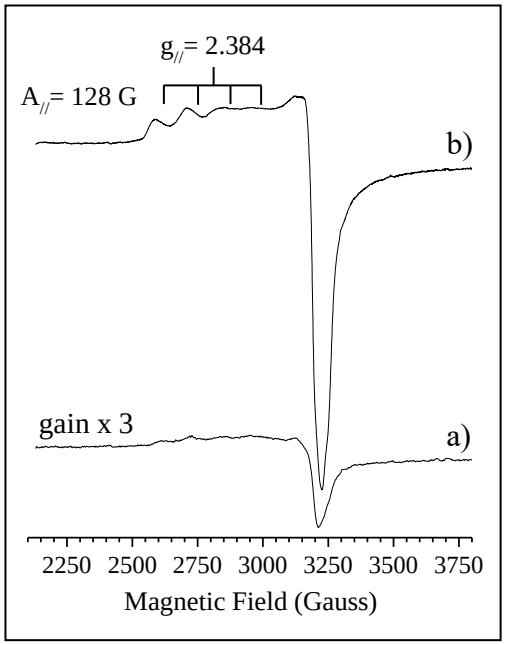

Figure 10. EPR spectra at a) 298 K and b) 130K of Cu_xO/SiO_2 matrix

The EPR spectrum of as-prepared Cu_xO/SiO_2 recorded at 298 K (Fig. 10a) shows a broad anisotropic signal, with tetragonal symmetry, attributable to d^9 Cu(II) centers [57]. The hyperfine coupling interaction with the copper nucleus is not well resolved.

In order to get more detailed information on the paramagnetic centers, the spectrum has been acquired at 130 K (Fig. 10b). In this case, both the crystal field symmetry and the hyperfine interaction with the copper nucleus (I=3/2) are well defined: $g_{//}$ = 2.384 and $g_{\perp}$ = 2.071 and $A_{//}$ = 128 G. By comparing the magnetic tensor values with those of several CuO_4 chromophores, an octahedral distorted symmetry is evident. The $A_{//}$ value also agrees with the suggested symmetry [58, 59]. These results are in accordance with the copper coordination derived from UV-Vis DRS.

The amount of paramagnetic Cu(II) centers, estimated from EPR spectra of samples containing known concentrations of Cu(II) ions resulted much lower (i.e. 0.12 ± 0.01 wt. %) than that derived from ICP-AES measurements (1.88 ± 0.02 wt.%). This may be associated to the magnetic coupling of copper centers probably due to their significant aggregation (see SEM and TEM investigation) and possibly to the presence of Cu(I) diamagnetic species.

Regarding the presence of Cu(I) centers, XPS investigation assessed that, though in a very low atomic amount, reduced copper species occur in the as-prepared catalyst (see Fig. 8). Moreover, further Cu(I) may form by partial reduction of Cu(II) during the vacuum annealing of Cu_xO/SiO_2 just before the interaction with the organic contaminants. This behavior has been recently demonstrated with XANES experiments carried out by Thibodeaux et al. [29] and it has been confirmed by EPR spectra of our Cu_xO/SiO_2 samples treated at 503 K under $p < 10^{-1}$ mbar. A

depletion of the intensity of the copper resonances is evident (Fig. S2, Supporting Information), suggesting that a thermal reduction of Cu(II) to Cu(I) actually takes place.

These results support the theoretical mechanism reported in Scheme 1, which predicts a key role for Cu(I) in the generation of highly active copper superoxide species fostering the oxidation of benzene.

The benzene contact with Cu_xO/SiO_2 has been performed by following an experimental procedure similar to that exploited by Dellinger et al. [10] for monitoring the EPFRs and ROS after adsorption of substituted aromatic compounds. Firstly, Cu_xO/SiO_2 sample was heated up 503 K under vacuum ($p < 10^{-1}$ mbar), then exposed to benzene vapors (20 mbar) at the same temperature. After contact, the powders were evacuated to $p < 10^{-1}$ mbar and the EPR spectra recorded.

The EPR spectrum of Cu_xO/SiO_2 recorded under $p < 10^{-1}$ mbar after benzene contact at 503 K shows an intensity decrease of the Cu(II) resonances and the presence of a new weak isotropic signal at $g = 2.0030$ (see magnification in the right-side of Fig. 11), which is highly stable and undergoes a noticeable decay only after 24 hours. This behaviour is typical of an Environmentally Persistent Free Radical (EPFR).

Based on the g value, we assigned the weak signal at $g = 2.0030$ to $PhenO^{\bullet}$ radicals deriving from benzene oxidation. No hyperfine interaction with copper nucleus was observed (Fig. 11), suggesting that the phenoxy radical is stabilized by interactions with the oxide and not with the copper centers.

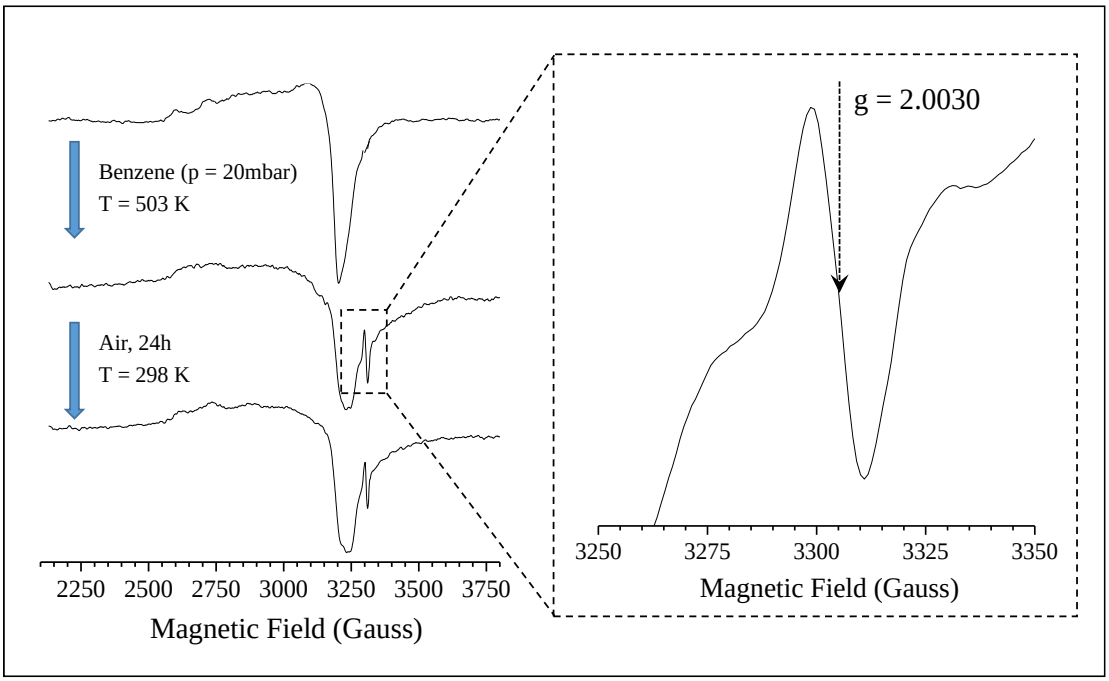

Figure 11. EPR spectra at 298 K of Cu_xO/SiO_2 before and after contact with benzene (p = 20 mbar) at 503 K. Right-side: magnification of the spectral region of EPFR species.

This outcome is in agreement with the substantially barrier-less dissociation of the intermediate **A5**, which provides the van der Waals adduct **A6** (- 49.9 kcal mol^{-1}) between the PhenO$^{\bullet}$ and the catalytic center (see Figure 1).

The decrease in copper(II) signal intensity after benzene contact, can be associated to the partial interaction of PhenO$^{\bullet}$ radical with Cu(II) paramagnetic centers owing to antiferromagnetic coupling. This leads to a quenching of the EPR signal, as similarly observed by Tolman et al.[60] for Cu(II)-phenoxy compounds.

Our results show that the EPFRs generation from benzene displays a lower yield in comparison to that of processes involving substituted aromatic rings [10, 11]. This result can be explained considering the higher stability of the benzene substrate and the absence of any activating group (e.g. ─OH, ─Cl, etc.). Moreover, it must be observed that only the Cu(II) isolated species, which account for < 0.1 wt. % of the total copper present in the catalyst, seem to be involved in promoting the formation of PhenO$^{\bullet}$ and, in turn, of phenol.

This supports the low amount of EPFRs detected and suggests, in agreement with Tsuruya et al.[34], that the other copper species, organized in Cu_xO nanoaggregates uniformly decorating silica surfaces (See SEM and TEM investigation), favor the fast oxidation of benzene to CO_2 and/or CO.

Finally, it must be observed that the mild vacuum applied on the sample before and after benzene exposure, may provide the O_2 amount suitable for driving the oxidation toward phenol. To prove this hypothesis, the contact procedure was initially carried out under high vacuum conditions ($p < 10^{-6}$ mbar), i.e. nearly in the absence of oxygen. After benzene interaction, no change in the EPR spectra of Cu_xO/SiO_2 in terms of EPFRs generation was noticeable (spectra not reported). This seems to confirm, in agreement with the theoretical mechanism in Scheme 1, that the formation of PhenO$^{\bullet}$ and, in turn, of phenol after the exposure to benzene vapors, actually needs the presence of a small amount of molecular oxygen which receives electrons from Cu(I) centers, producing Cu(II)-O_2^- species [38] attacking the stable aromatic ring.

As stated in Section 1, EPFRs can generate, in aqueous media, reactive oxygen species (ROS). Coherently, the mechanism described above predicts the dissociation of the intermediate **A5** into

PhenOH and hydroxyl radical species (OH•). In order to prove these steps, the generation of OH• radicals in aqueous solution by benzene-contacted Cu_xO/SiO_2 (EPFRs-containing particles) was tracked by spin-trap technique, using DMPO as spin-trap agent. Control experiments were also performed in the presence of Cu_xO/SiO_2 NPs before benzene adsorption (non-containing EPFRs).

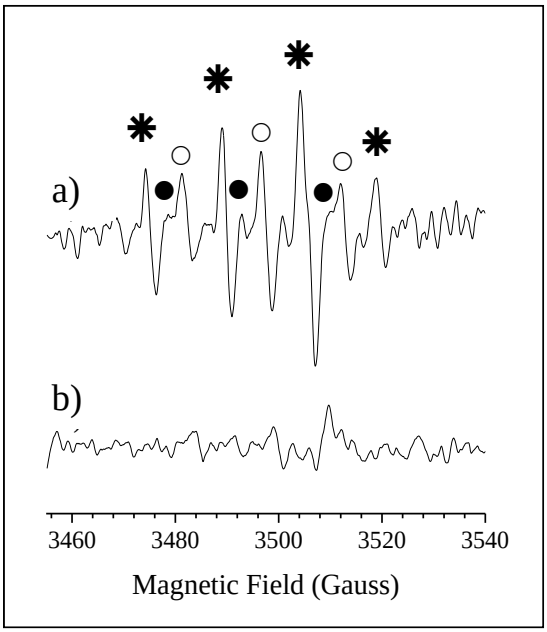

Figure 12. Comparison between the EPR spectra of suspensions of: a) Cu_xO/SiO_2 contacted with benzene (EPFRs-containing particles) and b) Cu_xO/SiO_2 before benzene adsorption (non-containing EPFRs particles).

EPR spectrum of EPFRs-containing particles (Fig. 12a) shows the signal of the DMPO-OH adduct (✱), with Hamiltonian fine interaction g = 2.0057 and hyperfine coupling constants with Hβ and N nuclei a_N = 14.9 G $a_{H\beta}$ = 14.9 G, in agreement with a very large number of references.

Less intense resonances related to free nitroxide species (○) (possibly deriving from DMPO oxidation [61], or side adducts with carbon-base radicals [62], DMPO dimerization [63], ring opening [62, 64], oxidation of hydroxylamines impurities [63]) can be also detected. Conversely, almost no signals have been detected for the sample before contact (Fig. 12b).

In summary, all these results support the theoretical mechanism reported in Figure 1, indicating that the interaction of benzene with copper centers in Cu_xO/SiO_2 leads to the formation of EPFRs and, in turn, to ROS species.

CONCLUSIONS

The present study reports on the comprehensive computational and experimental assessment of the EPFRs and ROS generation from benzene oxidation, catalyzed by highly porous Cu_xO/SiO_2 (x =1, 2), which simulates the combustion particulate matter (PM).

The computational approach, represented by both a cluster and a periodic surface model of Cu(I) centers, allowed to propose a reaction mechanism in which Cu(I) promotes the activation of molecular oxygen by forming a Cu(II)-O_2^-. This species, reacting with benzene, yields a Cu(II)-phenoxy complex that, upon an essentially barrier-less dissociation, gives a phenoxy radical stabilized by interaction with the catalyst. In the last step, dissociation of the OH radical recovers the catalyst, with concomitant reduction of Cu(II) to Cu(I).

Several experimental evidences support this mechanism.

XPS analysis of the Cu_xO/SiO_2 powders highlights the presence of Cu(I) species. Moreover, further Cu(I) may form by partial reduction of Cu(II) during the vacuum annealing of Cu_xO/SiO_2

just before the interaction with benzene, as confirmed by EPR spectra of Cu_xO/SiO_2 samples treated at 503 K under $p < 10^{-1}$ mbar.

The EPR spectrum of Cu_x/SiO_2 exposed to benzene in the presence of low O_2 pressure, shows the formation of a persistent phenoxy radical, whose stability should be ascribed to the interaction with the oxide and not with the metal center.

Finally, EPR spin-trap technique assesses the generation of $OH^{\cdot}$ radicals, as predicted by the theoretical model.

In conclusion, a convincing pathway for the oxidation of benzene and production of EPFRs, under catalysis of copper oxide supported on silica, has been here proposed based on computational and experimental results. These evidences highlight that the oxidation of unsubstituted aromatic hydrocarbons catalyzed by copper oxides promotes the formation of ROS, which elicit environmental and health damages either directly or as intermediates in formation of micropollutants.

AUTHOR INFORMATION

Corresponding Authors

*e-mail: massimiliano.darienzo1@unimib.it; ugo.cosentino@unimib.it

ASSOCIATED CONTENT

Supporting Information

Additional information concerning on computational models results and EPR investigation are included. This material is available free of charge via the Internet at http://pubs.acs.org.

ACKNOWLEDGMENTS

The computational resources from the CINECA (HPC Project mBI16_AmbCo) are gratefully acknowledged.

M.D. gratefully thanks Prof. Stefano Polizzi for the support in TEM investigation.

M.P. and A.B.M.G. kindly acknowledge the computing resources and the related technical support provided by CRESCO/ENEAGRID High Performance Computing infrastructure and its staff [65]; CRESCO/ENEAGRID High Performance Computing infrastructure is funded by ENEA, see http://www.cresco.enea.it/english for information.

REFERENCES

[1] Weber, R. Relevance of PCDD/PCDF formation for the evaluation of POPs destruction technologies − Review on current status and assessment gaps. *Chemosphere* **2007**, *67*, S 109–117.

[2] (a) Grandesso, E.; Ryan, S.; Gullett, B.; Touati, A.; Collina, E.; Lasagni, M.; Pitea, D. Kinetic modeling of polychlorinated dibenzo p dioxin and dibenzofuran formation based on carbon degradation reactions. *Environ. Sci. Technol.* **2008**, *42*, 7218-7224. (b) Cosentino, U.; Pitea, D.;

Moro, G. Computational modelling of de novo synthesis of Dibenzofuran: oxidative pathways of Pyrene and Benzodibenzofuran. *Theor. Chem. Acc*. **2012**, *131*, 1–12.

[3] Huang, H.; Buekens, A. De novo synthesis of polychlorinated Dibenzo-p-Dioxins and dibenzofurans. Proposal of a mechanistic scheme. *Sci. Total Environ.* **1996**, *193*, 121–141.

[4] Lenoir, D.; Wehrmeier, A.; Schramm, K.-W.; Kaune, A.; Zimmermann, R.; Taylor, P. H.; Sidhu, S. S. Thermal formation of polychlorinated dibenzo-p-dioxins and –furans: Investigation on relevant pathways. *Environ. Eng. Sci.* **1998**, 15, 37–47.

[5] Dellinger, B.; D'Alessio, A.; D'Anna, A.; Ciajolo, A.; Gullett, B.; Henry, H.; Keener M.; Lighty J.; Lomnicki S.; Lucas D. et al. Combustion Byproducts and Their Health Effects: Summary of the 10th International Congress. *Environmental Engineering Science* **2008** *25*, 1107–1114.

[6] Lomnicki, S.; Truong, H.; Vejerano, E.; Dellinger, B. Copper Oxide-Based Model of Persistent Free Radical Formation on Combustion-Derived Particulate Matter. *Environ. Sci. Technol.* **2008,** *42,* 4982–4988.

[7] Kiruri, L. W.; Khachatryan, L.; Dellinger, B.; Lomnicki, S. Effect of Copper Oxide Concentration on the Formation and Persistency of Environmentally Persistent Free Radicals (EPFRs) in Particulates. *Environ. Sci. Technol.* **2014**, *48*, 2212−2217.

[8] Kelley, M. A.; Hebert, V. H.; Thibeaux, T. M.; Orchard, M. A.; Hasan, F.; Cormier, S. A.; Thevenot, P. T.; Lomnicki, S. M.; Varner, K. J.; Dellinger, B. et al. Model Combustion-Generated Particulate Matter Containing Persistent Free Radicals Redox Cycle to Produce Reactive Oxygen Species. *Chem Res Toxicol*. **2013**, *26*, 1862–1871.

[9] Truong, H.; Lomnicki, S.; Dellinger, B. Potential for Misidentification of Environmentally Persistent Free Radicals as Molecular Pollutants in Particulate Matter. *Environ. Sci. Technol.* **2010,** *44,* 1933–1939.

[10] Khachatryan, L.; Vejerano, E.; Lomnicki, S.; Dellinger, B. Environmentally Persistent Free Radicals (EPFRs). 1. Generation of Reactive Oxygen Species in Aqueous Solutions. *Environ. Sci. Technol.* **2011**, *45*, 8559–8566.

[11] Khachatryan, L.; Dellinger, B. Environmentally Persistent Free Radicals (EPFRs)-2. Are Free Hydroxyl Radicals Generated in Aqueous Solutions? *Environ. Sci. Technol.* **2011**, *45*, 9232–9239

[12] Vejerano, E.; Lomnicki, S.; Dellinger, B. Formation and Stabilization of Combustion-Generated Environmentally Persistent Free Radicals on an $Fe(III)_2O_3$/Silica Surface. *Environ. Sci. Technol.* **2011**, *45*, 589–594.

[13] Vejerano, E.; Lomnicki, S. M.; Dellinger, B. Formation and Stabilization of Combustion-Generated, Environmentally Persistent Radicals on Ni(II)O Supported on a Silica Surface. *Environ. Sci. Technol.* **2012**, *46*, 9406– 9411.

[14] Vejerano, E.; Lomnicki, S.; Dellinger, B. Lifetime of Combustion-Generated Environmentally Persistent Free Radicals on Zn(II)O and Other Transition Metal Oxides. *J. Environ. Monit.* **2012**, *14*, 2803–2806.

[15] Patterson, M. C.; Keilbart, N. D.; Kiruri, L. W.; Thibodeaux, C. A.; Lomnicki, S.; Kurtz, R. L.; Poliakoff, E. D.; Dellinger, B.; Sprunger, P. T. EPFR Formation from Phenol Adsorption on Al_2O_3 and TiO_2: EPR and EELS Studies. *J. Chem. Phys.* **2013,** *422*, 277–282.

[16] Farquar, G. R.; Alderman, S. L.; Poliakoff, E. D.; Dellinger, B. X-Ray Spectroscopic Studies of the High Temperature Reduction of Cu(II)O by 2- Chlorophenol on a Simulated Fly Ash Surface. *Environ. Sci. Technol.* **2003**, *37*, 931–935.

[17] Assaf, N. W.; Altarawneh M.; Oluwoye, I.; Radny, M.; Lomnicki, S. M. and Dlugogorski, B. Z. *Environ. Sci. Technol.* **2016**, *50*, 11094-11102.

[18] Mosallanejad, S; Dlugogorski, B. Z.; Kennedy, E. M.; Stockenhuber, M.; Lomnicki, S. M.; Assaf, N. W.; Altarawneh M. *Environ. Sci. Technol.* **2016**, *50*, 1412-1418.

[19] Sauvain, J.-J.; Rossi, M. J.; Riediker, M. Comparison of Three Acellular Tests for Assessing the Oxidation Potential of Nanomaterials. *Aerosol Sci. Technol.* **2013**, 47, 218–227.

[20] Foucaud, L.; Wilson, M. R.; Brown, D. M.; Stone, V. Measurement of reactive species production by nanoparticles prepared in biologically relevant media. *Toxicol. Lett.* **2007**, *174*, 1–9.

[21] Schweigert, N.; Acero, J. L.; von Gunten U.; Canonica, S.; Zehnder, A. J.; Eggen, R. I. DNA degradation by the mixture of copper and catechol is caused by DNA-copper-hydroperoxo complexes, probably DNA-Cu(I)OOH. *Environ. Mol. Mutagen.* **2000**, *36*, 1, 5–12.

[22] Li, Y.; Trush, M. A. Reactive oxygen-dependent DNA damage resulting from the oxidation of phenolic compounds by a copper-redox cycle mechanism. *Cancer Res.* **1994**, *54*, 7 Suppl, 1895s–1898s.

[23] Pryor, W. A. Oxy-radicals and related species: Their formation, lifetimes, and reactions. *Annu. Rev. Physiol.* **1986**, *48*, 657–667.

[24] Sun, Q.; Altarawneh, M.; Dlugogorski, B. Z.; Kennedy, E. M.; Mackie, J. C. Catalytic Effect of CuO and Other Transition Metal Oxides in Formation of Dioxins: Theoretical Investigation of Reaction Between 2,4,5-Trichlorophenol and CuO. *Environ. Sci. Technol.* **2007**, *41*, 5708–5715.

[25] Altarawneh, M.; Dlugogorski, B. Z.; Kennedy, E. M.; Mackie, J. C. Mechanisms for formation, chlorination, dechlorination and destruction of polychlorinated dibenzo-p-dioxins and dibenzofurans (PCDD/Fs). *Progress in Energy and Combustion Science* **2009**, *35*, 245–274.

[26] Altarawneh, M.; Radny, M. W.; Smith, P. V.; Mackie, J. C.; Kennedy, E. M.; Dlugogorski, B. Z.; Soon, A.; Stampfl, C. A first-principles density functional study of chlorophenol adsorption on Cu_2O(110):CuO. *The Journal of Chemical Physics* **2009**, *130*, 184505–184507.

[27] Altarawneh, M.; Radny, M. W.; Smith, P. V.; Mackie, J. C.; Kennedy, E. M.; Dlugogorski, B. Z. Adsorption of chlorophenol on the Cu(1 1 1) surface: A first-principles density functional theory study. *Applied Surface Science* **2008**, *254*, 4218–4224.

[28] Altarawneh, M.; Carrizo, D.; Ziolkowski, A. Kennedy, E. M.; Dlugogorski, B. Z. Pyrolysis of permethrin and formation of precursors of polychlorinated dibenzo-p-dioxins and dibenzofurans (PCDD/F) under non-oxidative conditions. *Chemosphere* **2009**, *74*, 1435–1443.

[29] Thibodeaux, C. A.; The electronic structure of environmentally persistent free radicals formed on metal oxide surfaces. PhD dissertation, McNeese State University, 2015.

[30] Alderman, S. L.; Farquar, G. R.; Poliakoff, E. D.; Dellinger, B. An Infrared and X-Ray Spectroscopic Study of the Reactions of 2-Chlorophenol, 1,2-Dichlorobenzene, and

Chlorobenzene with Model CuO/Silica Fly Ash Surfaces. *Environ. Sci. Technol.* **2005**, *39*, 7396–7401.

[31] Kiruri, L. W.; Khachatryan, L.; Dellinger, B.; Lomnicki, S. Effect of Copper Oxide Concentration on the Formation and Persistency of Environmentally Persistent Free Radicals (EPFRs) in Particulates. *Environ. Sci. Technol*. **2014**, *48*, 2212–2217.

[32] Kehrer, J. P. The Haber-Weiss reaction and mechanisms of toxicity. *Toxicology* **2000**, *149*, 43–50.

[33] Yamanaka, H.; Hamada, R.; Nibuta, H.; Nishiyama, S.; Tsuruya, S. *Journal of Molecular Catalysis A* **2002**, *178*, 89-95.

[34] Hamada, R.; Shibata Y.; Nishiyama, S.; Tsuruya, Phys. Chem. Chem. Phys. **2003**, *5*, 956-965.

[35] Shibata, Y.; Hamada, R.; Ueda, T.; Ichihashi, Y. Nishiyama, S.; Tsuruya, S. Gas-Phase Catalytic Oxidation of Benzene to Phenol over Cu-Impregnated HZSM-5. Catalysts *Ind. Eng. Chem. Res.* **2005**, *44*, 8765-8772.

[36] Ichihashi, Y.; Kamizaki, Y.-H.; Terai, N.; Taniya, K.; Tsuruya, S.; Nishiyama, S. One-Step Oxidation of Benzene to Phenol over Cu/Ti/HZSM-5. Catalysts *Catal Lett*. **2010**, *134*, 324-329.

[37] Okemoto, A.; Tsukano, Y.-H.; Utsunomiya, A.; Taniya, K.; Ichihashi, Y.; Nishiyama, S. Selective catalytic oxidation of benzene over Cu/Ti/HZSM-5 under low oxygen pressure for one step synthesis of phenol. *J. Mol. Catal. A* **2016**, *411*, 372-376.

[38] Ene, A.B.; Archipov, T.; Roduner, E. Competitive Adsorption and Interaction of Benzene and Oxygen on Cu/HZSM5 Zeolites. *J. Phys. Chem. C* **2011**, *15*, 3688-3694.

[39] Tabler, A.; Häusser, A.; Roduner, E. Aerobic one-step oxidation of benzene to phenol on copper exchanged HZSM5 zeolites: A mechanistic study. *J. Mol. Catal. A* **2013**, *379*, 139-145.

[40] Gaussian 09, Revision D.01, M. J. Frisch, G. W. Trucks, H. B. Schlegel, G. E. Scuseria, M. A. Robb, J. R. Cheeseman, G. Scalmani, V. Barone, B. Mennucci et al. Gaussian, Inc., Wallingford CT, 2013.

[41] Becke, A. D. Density-functional thermochemistry III. The role of exact exchange. *J. Chem.* Phys **1993**, *98*, 5648-5652.

[42] Lee, C.; Yang, W. and Parr, R. G. Development of the Colle-Salvetti correlation-energy formula into a functional of the electron density. *Phys. Rev. B*, **1988**, *37*, 785-789.

[43] Miehlich, B.; Savin, A.; Stoll, H. and Preuss, H. Results obtained with the correlation-energy density functionals of Becke and Lee, Yang and Parr. *Chem. Phys. Lett.*, **1989**, *157*, 200-206.

[44] Hay, P. J. and Wadt, W. R. Ab initio effective core potentials for molecular calculations – potentials for the transition-metal atoms Sc to Hg. *J. Chem. Phys.* **1985**, *82*, 270-283.

[45] Hay, P. J. and Wadt, W. R. Ab initio effective core potentials for molecular calculations – potentials for main group elements Na to Bi. *J. Chem. Phys.* **1985**, *82*, 284-98.

[46] Hay, P. J. and Wadt, W. R. Ab initio effective core potentials for molecular calculations – potentials for K to Au including the outermost core orbitals. *J. Chem. Phys.* **1985**, *82*, 299-310.

[47] Menon, A.S.; Radom, L. Consequences of Spin Contamination in Unrestricted Calculations on Open-Shell Species: Effect of Hartree−Fock and Møller−Plesset Contributions in Hybrid and

Double-Hybrid Density Functional Theory Approaches. *J. Phys. Chem. A* **2008**, *112*, 13225-13230.

[48] Kresse, G.; Joubert, D. From Ultrasoft Pseudopotentials to the Projector Augmented-Wave Method. *Phys. Rev. B* **1999**, *59*, 1758− 1775.

[49] J. P. Perdew, K. Burke, and M. Ernzerhof. Generalized gradient approximation made simple. *Phys. Rev. Lett.*, **1996**, ***77*,** 3865-3868.

[50] J. P. Perdew, K. Burke, and M. Ernzerhof. Erratum: Generalized gradient approximation made simple. *Phys. Rev. Lett.* **1997**, *78*, 1396.

[51] Dudarev, S. L.; Botton, G. A.; Savrasov, S. Y.; Humphreys, C. J.; Sutton, A. P. Electron-Energy-Loss Spectra and the Structural Stability of Nickel Oxide: An LSDA+U Study. *Phys. Rev. B* **1998**, *57*, 1505− 1509.

[52] Iseroff Bendavid, L.; Carter, E. A. CO_2 adsorption on Cu_2O (111): A DFT+U and DFT+D study. *J. Phys. Chem. C*, **2013**, *117*, 26048–26059.

[53] Kaushik, V. K. Identification of oxidation states of copper in mixed oxides and chlorides using ESCA. *Spectrochimica Acta B* **1989**, *44*, 581-587.

[54] Goodman, B. R.; Schneider, W. F. Hass, K. C. Theoretical analysis of oxygen-bridged Cu pairs in Cu-exchanged zeolites. *Catalysis Letter* **1998**, *56*, 183-188.

[55] Goodman, B. R.; Hass K. C.; Schneider W. F.; Adams J. B. Cluster Model Studies of Oxygen-Bridged Cu Pairs in Cu−ZSM-5 Catalysts. *J. Phys. Chem. B* **1999**, *103*, 10452-10460.

[56] Wagner, C. D.; Riggs, W. M.; Davis, L. E.; Moulder J. F.; Muilenberg G. E. *Handbook of X-Ray Photoelectron Spectroscopy;* Eds. Perkin-Elmer Corporation: Eden Prairie, MN, 1979.

[57] Velu, S.; Wang, L.; Okazaki, M.; Suzuki, K.; Tomura, S. Characterization of MCM-41 mesoporous molecular sieves containing copper and zinc and their catalytic performance in the selective oxidation of alcohols to aldehydes. *Microporous and Mesoporous Materials* **2002**, *54*, 113–126.

[58] Solomon, E. I; Baldwin, M. J.; Lowery, M. D. Electronic structures of active sites in copper proteins: contributions to reactivity. *Chem. Rev.* **1992**, *92*, 521-542.

[59] Soria, J.; Martínez-Arias, A.; Martínez –Chaparro, A.; Conesa, J. C.; Schay, Z. Influence of the Preparation Method, Outgassing Treatment, and Adsorption of NO and/or O_2 on the Cu^{2+} Species in Cu-ZSM-5: An EPR Study. *Journal of Catalysis,* **2000**, *190*, 352-363.

[60] Halfen J. A. Jazdzewski B. A.; Mahapatra S.; Berreau L. M.; Wilkinson E. C.; Que L. Jr.; Tolman W. B. Synthetic Models of the Inactive Copper(II)−Tyrosinate and Active Copper(II)−Tyrosyl Radical Forms of Galactose and Glyoxal Oxidases. *J. Am. Chem. Soc.* **1997,** *119*, 8217-8227.

[61] Makino, K.; Hagi, A.; Ide, H.; Murakami, A.; Nishi, M. Mechanistic studies on the formation of aminoxyl radicals from 5,5-dimethyl-1-pyrroline-N-oxide in Fenton systems. Characterization of key precursors giving rise to background ESR signals. *Can. J. Chem*. **1992**, *70*, 2818-2827.

[62] Mottley, C.; Mason, R. P. Biological Magnetic Resonance: Spin labeling, Theory and applications Ed. Berliner, L. J.; Reuben, J.; Springer, 1989.

[63] Michail, K.; Siraki, A. G. Post-Trapping Derivatization of Radical-Derived EPR-Silent Adducts: Application to Free Radical Detection by HPLC/UV in Chemical, Biochemical, and Biological Systems and Comparison with EPR Spectroscopy. *Anal. Chem.* **2012**, *84*, 6739−6746.

[64] Bilski, P.; Reszka, K.; Bilska, M.; Chignell, C. F. Oxidation of the Spin Trap 5,5-Dimethyl-1-pyrroline N-Oxide by Singlet Oxygen in Aqueous Solution. *J. Am. Chem. Soc.* **1996**, *118*, 1330-1338.

[65] G. Ponti *et al.*, "The role of medium size facilities in the HPC ecosystem: the case of the new CRESCO4 cluster integrated in the ENEAGRID infrastructure", *Proceedings of the 2014 International Conference on High Performance Computing and Simulation, HPCS*, **2014**, *art. n. 6903807*, 1030-1033.

TOC graphic